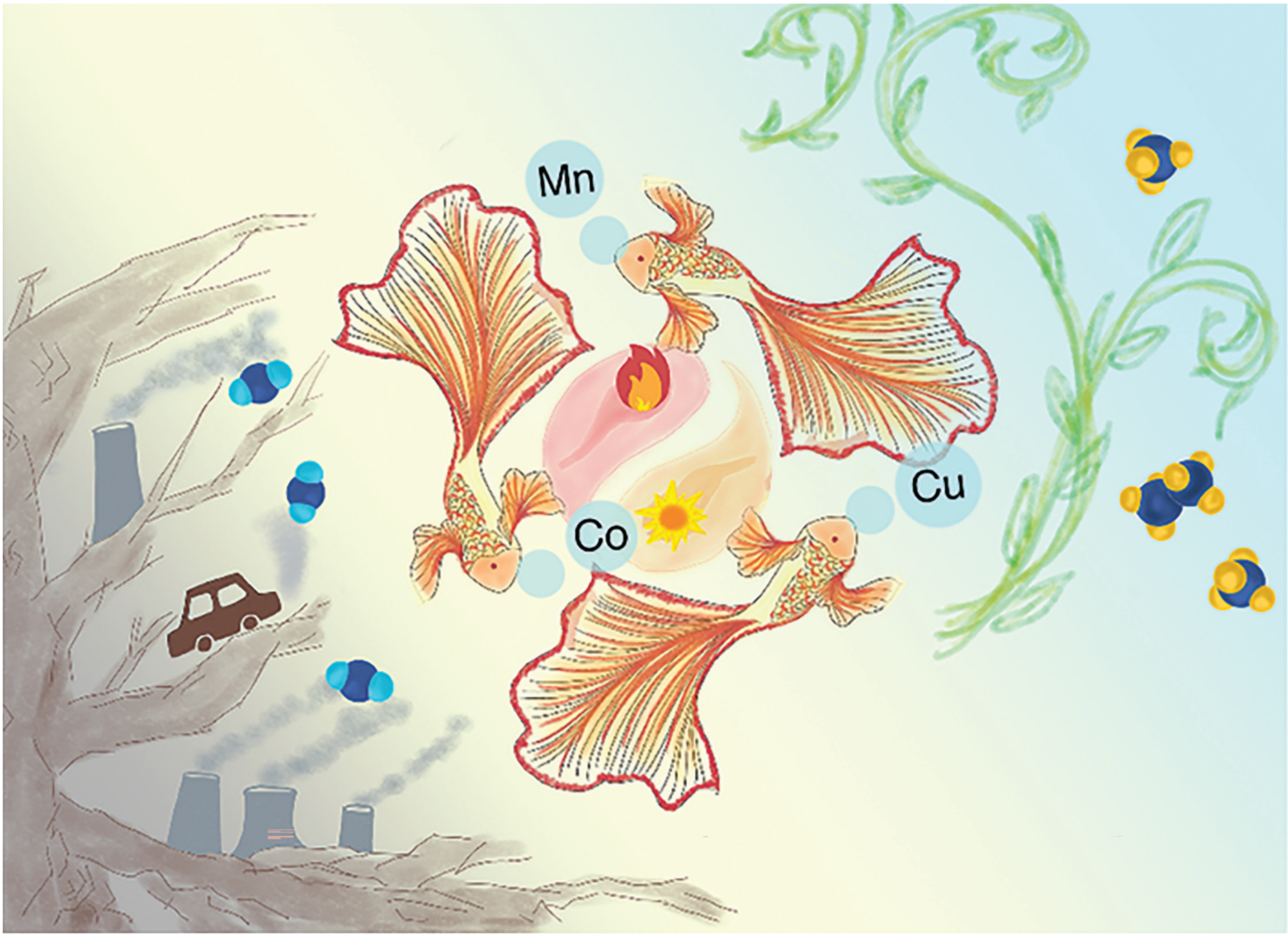

**An article presented by Professor Zhen-Hong He and Professor Zhao-Tie Liu from Shaanxi University of Science and Technology and Shaanxi Normal University, China.**

Photothermal $CO_2$ hydrogenation to hydrocarbons over trimetallic Co–Cu–Mn catalysts

Photocatalytic $CO_2$ reduction is a highly vital process for converting $CO_2$ into valuable chemicals. However, the reaction always proceeds less efficaciously at low temperature. The combination of photo and thermal conditions is one of feasible approaches to achieve the reaction with high efficiency and has gained much attention recently. In the present work, trimetallic Co–Cu–Mn catalysts were developed in photothermal $CO_2$ hydrogenation to $CH_4$ and $C_{2+}$ hydrocarbons. The structural and photoelectric characteristics, as well as adsorption behaviors of these catalysts affected the catalytic performances remarkably.

## As featured in:

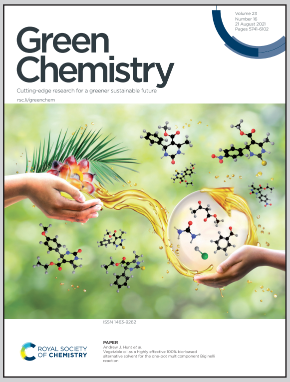

See Zhen-Hong He, Zhao-Tie Liu *et al.*, *Green Chem.*, 2021, **23**, 5775.

ROYAL SOCIETY OF CHEMISTRY

rsc.li/greenchem

Green Chemistry

ROYAL SOCIETY OF CHEMISTRY

PAPER

View Article Online
View Journal | View Issue

Check for updates

**Cite this:** *Green Chem.*, 2021, **23**, 5775

# Photothermal $CO_2$ hydrogenation to hydrocarbons over trimetallic Co–Cu–Mn catalysts†

Zhen-Hong He, *[a] Zhu-Hui Li,[a] Zhong-Yu Wang,[a] Kuan Wang,[a] Yong-Chang Sun,[a] Sen-Wang Wang,[b] Wei-Tao Wang,[a] Yang Yang [a] and Zhao-Tie Liu *[a,b]

Received 4th April 2021,
Accepted 22nd June 2021

DOI: 10.1039/d1gc01152a

rsc.li/greenchem

Photocatalytic $CO_2$ reduction is a highly vital process for converting $CO_2$ into valuable chemicals. However, the reaction always proceeds less efficaciously at low temperature. A combination of optical and thermal conditions is one of the feasible approaches to achieve the reaction with high efficiency and has gained much attention recently. In the present work, we prepared several Co–Cu–Mn trimetallic catalysts *via* a simple co-precipitation method, which were used in catalyzing photothermal $CO_2$ reduction to hydrocarbons. The metal composition and reduction temperature of the catalysts had important effects on their structural and photoelectrical characteristics and adsorption behaviors, further resulting in diverse catalytic performances. Among the prepared trimetallic catalysts, $Co_7Cu_1Mn_1O_x$(200), with a Co/Cu/Mn molar ratio of 7/1/1 and reduced at 200 °C in $H_2$ for 2 h, could produce $CH_4$ with an activity of 14.5 mmol $g_{cat}^{-1}$ $h^{-1}$ in 10% $CO_2$/30% $H_2$/60% $N_2$, and $CH_4$ and $C_{2+}$ hydrocarbons with the activities of 15.9 and 7.5 mmol $g_{cat}^{-1}$ $h^{-1}$ in 25% $CO_2$/75% $H_2$, respectively. The present strategy for constructing trimetallic oxide catalysts for the photothermal reaction not only provides a highly active catalyst for $CO_2$ utilization, but also offers a potential possibility for reducing the high temperature of conventional thermal reactions.

## Introduction

$CO_2$ is the primary greenhouse gas, whose concentration in the atmosphere continues to rise.[1] It is also an important C1 source and can be converted into many valuable chemicals such as CO,[2] hydrocarbons,[3–5] olefins,[6] acids,[7–9] alcohols,[10–12] *etc*. Although many efforts have been invested in this area, it is still very difficult to convert $CO_2$ into chemicals due to its thermodynamic stability and chemical inertness.[1] $CO_2$ hydrogenation to hydrocarbons represents an essential and green way for its utilization.[13] However, the conventional thermal process is always conducted under harsh conditions, leading to the formation of carbon deposit, the increase of energy consumption, *etc*. The photocatalytic method is an ideal way for the reaction, which could be carried out under mild conditions and using solar energy. However, this route suffers from low activity especially at room temperature, impeding its further applications. Recently, the photothermal catalytic method has gained increasing attention, especially in $CO_2$ reduction.[14,15]

The photothermal routes always contain four types, including thermal-assisted photocatalysis, photo-assisted thermocatalysis, photothermal co-catalysis, and photo-driven thermocatalysis.[16] Generally, these routes combine the advantages of both photocatalysis and thermal catalysis including high activity, proceeding under mild conditions, efficient energy utilization, *etc*. To date, many catalysts such as Ru/silicon nanowire,[17] $RuO_2/SrTiO_3$,[18] $RuO_2$/3D silicon photonic crystals,[19] Ru@FL-LDHs (Ru/Mg–Al LDHs matrix),[20] $Ru/Al_2O_3$,[21] $Ru/TiO_2$,[22] $Pd@Nb_2O_5$,[23] CoFeAl-LDH nanosheet,[13] $Ni/SiO_2{\cdot}Al_2O_3$,[14] $Cu_2O$/Zn-MOF,[24] $Cu_2O$/graphene,[25] *etc*. have been used for photothermal $CO_2$ hydrogenation, and their catalytic performances are given in Table S1.† Significant advances have been made in recent years; however, most of the above catalysts suffer from drawbacks such as using expensive noble metals, working at high temperature, and exhibiting low activity. Besides, the obtained products mainly focused on C1 chemicals such as CO and $CH_4$. The synthesis of $C_{2+}$ products *via* a photothermal route is a more difficult but significant issue, which is rarely involved in the above developed catalytic systems.[26] Considering the above aspects, to develop a cost-efficient, highly active and reusable catalyst for photothermal

---

[a] Shaanxi Key Laboratory of Chemical Additives for Industry, College of Chemistry and Chemical Engineering, Shaanxi University of Science & Technology, 710021 Xi'an, China. E-mail: hezhenhong@sust.edu.cn, ztliu@snnu.edu.cn
[b] School of Chemistry & Chemical Engineering, Shaanxi Normal University, 710119 Xi'an, China

† Electronic supplementary information (ESI) available. See DOI: 10.1039/d1gc01152a

$CO_2$ reduction into $CH_4$ and $C_{2+}$ hydrocarbons is particularly important.

On the other hand, it has been well known that pure metals used in $CO_2$ hydrogenation always showed a low activity due to their low $CO_2$ binding capacity.[27] Oxides could not only anchor metal atoms but also provide vacancies for the reaction, and in this way, they could participate in the reaction and enhance the catalytic performances.[28] Trimetallic oxide catalysts show unique electronic and structural features different from their individual components. The complex composition of trimetallic catalysts could form multiple interfaces conducive to catalysis.[29] In this aspect, trimetallic catalysts have been widely used in many reactions such as CO and $CO_2$ hydrogenation,[30–32] ethanol steam reforming,[33] ammonia oxidation,[34] *etc.* with good performances. In particular, complicated metal–trimetallic oxides can provide many vacancies and active sites for catalysis, and have great potential for application in $CO_2$ reduction. Herein, a series of Co–Cu–Mn trimetallic oxides were prepared and used for photothermal $CO_2$ reduction, and the screened $Co_7Cu_1Mn_1O_x$(200) catalyst, with a Co/Cu/Mn ratio of 7/1/1 and reduced at 200 °C in $H_2$, showed a high $CH_4$ formation activity (14.5 mmol $g_{cat}^{-1}$ $h^{-1}$) even at low $CO_2$ (10%) and $H_2$ (30%) concentrations, which lies in the highest activity range in Table S1.† Interestingly, after increasing the $CO_2$ and $H_2$ concentrations to 25% and 75%, 15.9 and 7.5 mmol $g_{cat}^{-1}$ $h^{-1}$ of $CH_4$ and $C_{2+}$ hydrocarbons were produced with selectivities of 65.4% and 30.8%, respectively. Moreover, the catalyst has a good temporal stability under continuous-flow conditions. The metal/oxides were confirmed to be very important for the catalytic performance, in which the $Co^0$ species were the active sites, which together with the oxides acted as supports and semiconductors for providing a local heating environment *via* the photothermal effects. The Cu species could promote the reduction of Co and Mn oxides, and also promote the coupling of C–C bonds to produce $C_{2+}$ products especially at a high $CO_2$ concentration. The Mn species could on one hand enhance the adsorption of $CO_2$ and $H_2$, and also provide the photothermal effect to produce a local heating effect to promote the reaction. The present strategy for constructing trimetallic catalysts for the photothermal reaction does not only provide a simple but efficient way to convert $CO_2$ into valuable hydrocarbons, but also offer a general method for reducing the reaction temperature of conventional high-temperature reactions.

## Results and discussion

### Preparation and characterization of catalysts

Trimetallic Co–Cu–Mn catalysts were prepared by a simple coprecipitation method, and the details are given in the ESI.† The prepared catalysts were denoted as $Co_aCu_bMn_cO_x(T)$, in which $a/b/c$ and $T$ represent the Co/Cu/Mn molar ratio and the reduction temperature, respectively. $Co_aCu_bMn_cO_x$ means unreduced catalysts. The morphologies of the catalysts were examined by TEM tests. Initially, the $Co_7Cu_1Mn_1O_x$ catalyst mainly showed the morphology of nanoparticles with the size range of 6–15 nm (Fig. 1a and b). The lattice spacings of 0.186, 0.246, 0.219, 0.152, 0.197, and 0.135 nm in the HRTEM image

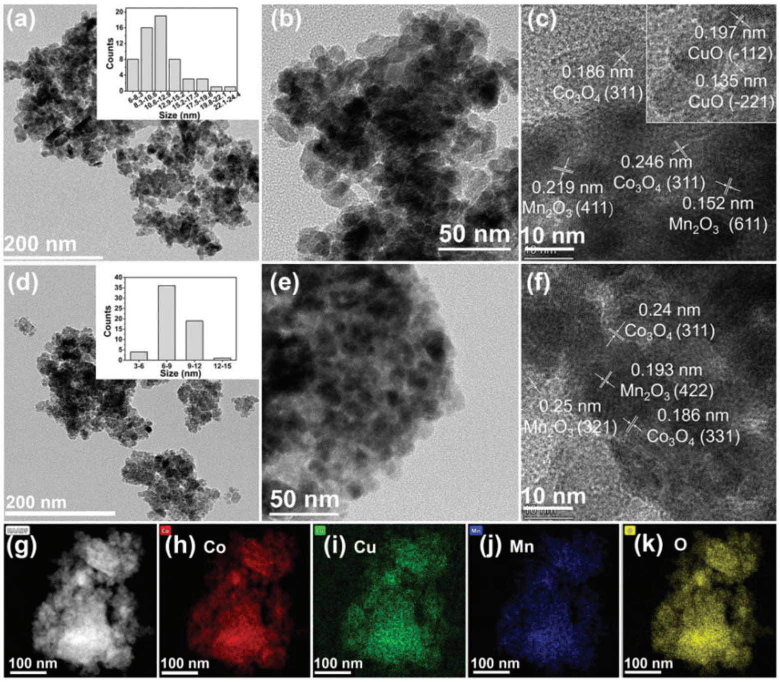

**Fig. 1** TEM images (a, b, d, and e) and HRTEM images (c and f) for the $Co_7Cu_1Mn_1O_x$ (a–c) and $Co_7Cu_1Mn_1O_x$(200) (d–f) catalysts, HAADF-STEM image for the $Co_7Cu_1Mn_1O_x$(200) catalyst (g) and the corresponding EDS elemental mapping of Co, Cu, Mn, and O (h–k). The insets in (a) and (d) are the size distribution histograms for the $Co_7Cu_1Mn_1O_x$ and $Co_7Cu_1Mn_1O_x$(200) catalysts.

could be successively indexed to the (331) and (311) planes of $Co_3O_4$, the (411) and (611) planes of $Mn_2O_3$, and the (−112) and (−221) planes of CuO (Fig. 1c).

After reduction, the $Co_7Cu_1Mn_1O_x$(200) catalyst maintained the nanoparticle morphology in the size range of 6–12 nm (Fig. 1d and e). $Co_3O_4$ and $Mn_2O_3$ were also detected, as shown in Fig. 1f. The HAADF-STEM and EDX elemental mappings of the $Co_7Cu_1Mn_1O_x$(200) catalyst showed that Co, Cu, Mn, and O elements are homogeneously dispersed over the whole grain (Fig. 1g to k).

For comparison, the TEM images of catalysts with different Co/Cu/Mn ratios were also studied, and the results are shown in Fig. S1.† With the increasing Co content, the morphology changed from nanosheets to nanoparticles. For example, the $Co_3Cu_1Mn_1O_x$(200) and $Co_5Cu_1Mn_1O_x$(200) catalysts were nanosheets, while the $Co_7Cu_1Mn_1O_x$(200) and $Co_9Cu_1Mn_1O_x$(200) catalysts were mainly nanoparticles, which were beneficial for exposing more active sites.

The molar ratios of the bimetallic and trimetallic catalysts were tested by ICP-OES, and the results are given in Table S2.† The molar ratios of metals were consistent with the feed amounts.

XRD examinations showed that all the tested unreduced catalysts such as $Co_7Cu_1Mn_1O_x$, $Co_7Mn_1O_x$, and $Co_7Cu_1O_x$ showed the XRD patterns of $Co_3O_4$ (JCPDS file no. 73-1701). No obvious $CuO_x$ or $MnO_x$ peaks were found, implying that they were easily incorporated into the $Co_3O_4$ crystals and were well dispersed (Fig. 2a). The $Co_7Cu_1Mn_1O_x$(200) catalyst showed the same peaks as that of the $Co_7Cu_1Mn_1O_x$ catalyst, but with lower intensities, indicating the crystallinity decrease of the $Co_3O_4$ component after reduction.

The XRD pattern of the $Co_7Cu_1Mn_1O_x$(200) catalyst was almost the same as that of the unreduced catalyst, and it is mainly attributed to the $Co_3O_4$ phase (Fig. 2b). However, two small peaks at 43.0° and 61.8° were carefully detected, which could be assigned to the CoO (200) and (220) planes (JCPDS file no. 70-2855). No $Co^0$, $Cu^0$, $Cu_2O$, or $Mn_2O_3$ species were detected due to their low amounts. The $Co_7Mn_1O_x$(200) catalyst showed three peaks at 36.8°, 42.7°, and 61.8°, which could be assigned to the CoO (111), (200), and (220) planes (JCPDS file no. 78-0431), respectively. Two phases of $Co^0$ fcc and hcp were identified in the $Co_7Cu_1O_x$(200) catalyst, and the formation of two phases is commonly observed in the synthesis of cobalt nanostructures.[35] The peaks at 41.5°, 44.4°, 47.4°, and 75.9° could be indexed to $Co^0$ hcp (100), (002), (101), and (110) facets (JCPDS file no. 01-071-4239), respectively. The peaks at 44.4° and 51.5° could be contributed to the $Co^0$ fcc (111) and (200) planes (JCPDS file no. 01-071-4651).[35] The results indicated that $Co_3O_4$ could be reduced to $Co^0$ by the promotion of Cu species, and this will be further verified by the following $H_2$-TPR tests. No $MnO_x$ or $CuO_x$ species were detected due to their good dispersion. It is worth noting that although Cu could promote the reduction of $CoO_x$ species to $Co^0$, no $Co^0$ was detected in the bulk phase of the $Co_7Cu_1Mn_1O_x$(200) catalyst.

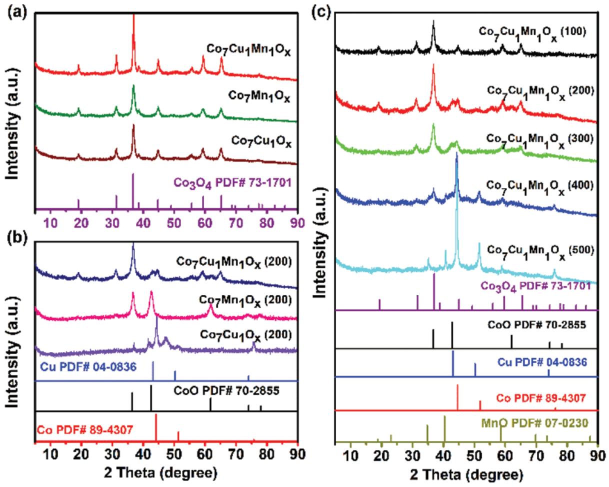

**Fig. 2** XRD patterns of (a) the unreduced $Co_7Mn_1O_x$, $Co_7Cu_1O_x$, and $Co_7Cu_1Mn_1O_x$ catalysts; (b) $Co_7Mn_1O_x$(200), $Co_7Cu_1O_x$(200), and $Co_7Cu_1Mn_1O_x$(200); and (c) $Co_7Cu_1Mn_1O_x$ catalysts reduced at different temperatures.

The XRD patterns of the catalysts with different Co/Cu/Mn ratios also showed the main peaks of $Co_3O_4$ and CoO (Fig. S2†); however, the $Co_3Cu_1Mn_1O_x$(200) and $Co_5Cu_1Mn_1O_x$(200) catalysts showed a wide peak at around 20°, indicating that they possess amorphous structures.

The results of the $N_2$ adsorption/desorption tests are shown in Fig. S3 and Table S3.† The reduction temperature affects the catalyst structure remarkably, and the BET surface areas of the tested trimetallic catalysts declined gradually with the increase of the reduction temperature, which is probably because the high reduction temperature leads to catalyst sintering. The bimetallic Co–Cu catalyst shows the lowest BET surface area, while the Co–Mn catalyst presents the highest. Indeed, the surface areas of the $CoO_x$ and $Co_7Cu_1Mn_1O_x$(100, 200, and 300) catalysts did not differ greatly from one another, thus their diverse performances did not stem from the difference in their surface areas.

To distinguish the valences of the Co, Cu, and Mn species on the surface of the catalysts, the XPS of Co 2p, Cu 2p, Mn 2p and 3s, and AES of Cu $L_3M_{4,5}M_{4,5}$ were analyzed (Fig. 3).[5,36,37] In the XPS of the $Co_7Cu_1Mn_1O_x$ catalyst, the Co element was composed of $Co^{3+}$ and $Co^{2+}$ species, which was confirmed by the peaks at 779.5 eV and 780.9 eV, which can be attributed to the $Co^{3+}$ and $Co^{2+}$ $2p_{3/2}$ peaks (Fig. 3a).[38] The $Cu^{2+}$ 2p XPS showed two peaks at 934.5 eV and 954.2 eV, which could be assigned to $Cu^{2+}$ $2p_{3/2}$ and $2p_{1/2}$, respectively (Fig. 3b and c). The XPS peaks of Co species in the $Co_7Cu_1Mn_1O_x$(200) catalyst were the same as those in the unreduced catalyst; however, the Cu species was found to be $Cu^+$. The Mn XPS indicated that the catalyst contains $Mn^{3+}$ oxidation state (Fig. 3d and e). The XPS results indicated that the surface of the $Co_7Cu_1Mn_1O_x$(200) catalyst mainly contained $Co^{2+}$, $Co^{3+}$, $Cu^+$, a small amount of $Cu^{2+}$, and $Mn^{3+}$, respectively, but no $Co^0$ or $Cu^0$ species were detected for air oxidation.

For comparison, the XPS spectra of the catalysts reduced at different temperatures were also tested. The Co element in these catalysts was mainly composed of $Co^{2+}$ and $Co^{3+}$ species

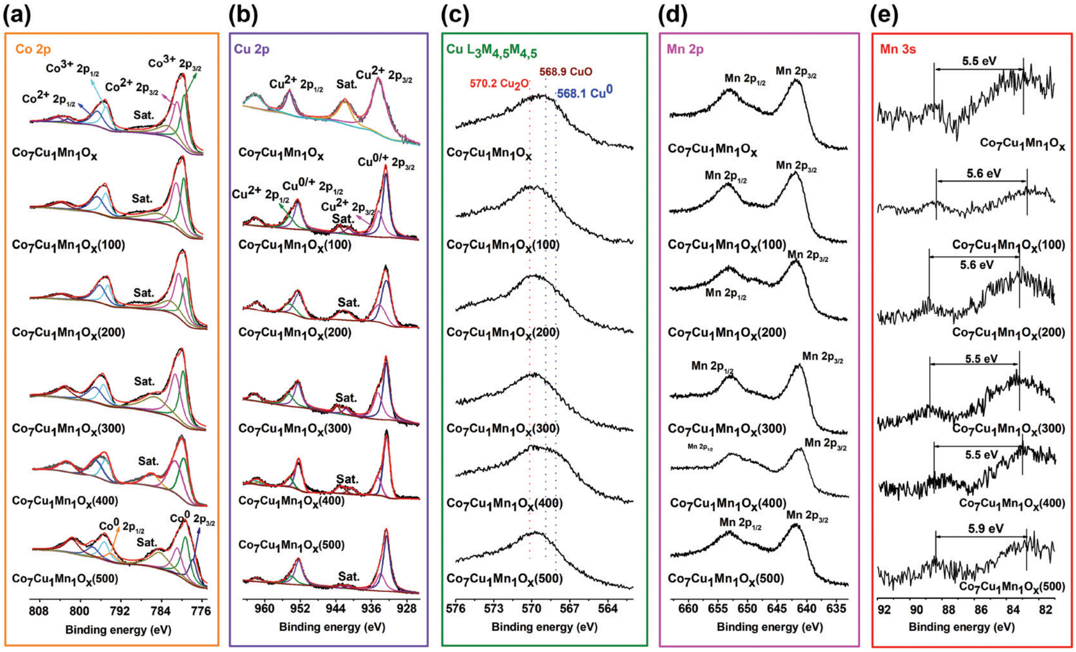

**Fig. 3** XPS spectra of the unreduced $Co_7Cu_1Mn_1O_x$ catalyst and the $Co_7Cu_1Mn_1O_x$(100, 200, 300, and 500) catalysts. (a) Co 2p XPS, (b) Cu 2p XPS, (c) Cu $L_3M_{4,5}M_{4,5}$ AES spectra, (d) Mn 2p XPS, and (e) Mn 3s XPS, respectively.

but with different contents. The $Co^{2+}$ component increased with the increase of the reduction temperature. No obvious $Co^0$ species was found until the reduction temperature reached 500 °C. As for the Cu XPS, the area of the satellite peak around 942 eV decreased with increasing reduction temperature, indicating that $Cu^{0/+}$ $2p_{3/2}$ increased. Besides, all the reduced catalysts possess the dominant $Cu^+$ component. The Mn 3s XPS showed that the $Co_7Cu_1Mn_1O_x$(500) catalyst is composed of $Mn^{2+}$ species, *i.e.*, MnO, while the others showed $Mn^{3+}$ species.

The XPS spectra of the Co–Cu–Mn trimetallic catalysts with different molar ratios were also investigated, and the results are given in Fig. S4.† All the elements had the same valences but contained different contents, such as $Co^{2+}$, $Co^{3+}$, $Mn^{3+}$, $Cu^+$, and a small amount of $Cu^{2+}$, which are similar to the $Co_7Cu_1Mn_1O_x$(200) catalyst, indicating that they are probably active in the reaction. This was confirmed by the following catalytic activity studies (Table 1).

The Raman spectrum of the $Co_7Cu_1Mn_1O_x$(200) catalyst showed a peak at 680 $cm^{-1}$, which could be assigned to the A1 g mode of $Co_3O_4$ (Fig. S5†).[39] This profile is similar to those of the $Co_7Cu_1Mn_1O_x$ and $Co_7Cu_1Mn_1O_x$ (100, 300, and 400) catalysts, indicating that $Co_3O_4$ exists in these catalysts. Interestingly, the $Co_7Cu_1Mn_1O_x$(500) catalyst showed a wide peak at 540 $cm^{-1}$, assigned to the one-phonon LO mode of CoO,[40] which was formed by the partial oxidation of $Co^0$ by local laser heating.[45] No obvious Cu or Mn species were detected, indicating that they have permeated into the $Co_3O_4$ crystal lattice.

The above characterization studies showed that the $Co_7Cu_1Mn_1O_x$(200) catalyst mainly possesses $Co_3O_4$ in the bulk phase, while the surface of the catalyst was composed of $Co^{3+}$, $Co^{2+}$, $Mn^{3+}$, $Cu^+$, and a small amount of $Cu^{2+}$ species, which are in the forms of $Co_3O_4$, $Mn_2O_3$, $Cu_2O$, and CuO. The catalysts reduced at 100, 200, and 300 °C, and the catalysts with different Co/Cu/Mn molar ratios contained similar components but of different concentrations, indicating that they possess similar structures and properties.

## Catalytic performances

Photothermal $CO_2$ hydrogenation was carried out in a tubular reactor (Fig. S6),† and the procedure details are given in the ESI.† The products of photothermal $CO_2$ reduction include CO, $CH_4$, and $C_{2+}$ hydrocarbons (mainly $C_2$ to $C_6$) in the present work. Initially, the catalytic performances over different catalysts are given in Table 1. No products were detected in the absence of a catalyst, and the sole metal catalysts or the bimetallic catalysts showed a very low activity in the reaction. The $Co_7Cu_1Mn_1O_x$(200) catalyst showed the best catalytic performances with a $CH_4$ formation activity of 14.5 mmol $g_{cat}^{-1}$ $h^{-1}$ and a selectivity of 85.3% (entries 1–7 *vs.* 8). These activities were achieved under the irradiation of a 300 W Xe lamp (234 mW $cm^{-2}$, 300–1100 nm) and heat generated by an additional electric heater (Fig. S6†). Unlike the $CuO_x$(200) and $MnO_x$(200) catalysts, the $CoO_x$(200) catalyst could show a very low $CH_4$ formation activity (only 3.1 mmol $g_{cat}^{-1}$ $h^{-1}$) (entries 2–4), demonstrating that the Co species is probably the active species, while the $CuO_x$ and $MnO_x$ species are the promoters for the Co species. Indeed, the Cu and Mn species are always used as promoters or active sites for the Co-catalyzed $CO_2$ reduction.[41] The activities of the bimetallic $Cu_1Mn_1O_x$ or $Co_7Mn_1O_x$ catalysts confirmed that Cu or Mn are not the active sites (entries 5–7). Interestingly, the $Co_7Cu_1O_x$(200) catalyst showed higher activities for the formation of $CH_4$ and $C_{2+}$

**Table 1** Photothermal $CO_2$ hydrogenation over diverse catalysts[a]

| | | | Activity[b] (mmol $g_{cat}^{-1}$ $h^{-1}$) | | | |
|---|---|---|---|---|---|---|
| Entry | Catalyst | Conv. (%) | $CH_4$ | $C_{2+}$ | CO | $CH_4$[b] Sele. (%) |
| 1 | None | 0 | 0 | 0 | 0 | — |
| 2 | $CoO_x(200)$ | 5.6 | 3.1 ± 0.1 | 0.4 ± 0.1 | 0 | 88.6 |
| 3 | $CuO_x(200)$ | 0 | 0 | 0 | 0 | — |
| 4 | $MnO_x(200)$ | 0 | 0 | 0 | 0 | — |
| 5 | $Cu_1Mn_1O_x(200)$ | 0 | 0 | 0 | 0 | — |
| 6 | $Co_7Mn_1O_x(200)$ | 0.8 | 0.2 ± 0.1 | 0 | 0.3 ± 0.1 | 40.0 |
| 7 | $Co_7Cu_1O_x(200)$ | 14.0 | 5.9 ± 0.2 | 2.4 ± 0.1 | 0.4 ± 0.1 | 67.8 |
| 8 | $Co_7Cu_1Mn_1O_x(200)$ | 27.4 | 14.5 ± 0.2 | 1.4 ± 0.1 | 1.1 ± 0.1 | 85.3 |
| 9 | $Co_3Cu_1Mn_1O_x(200)$ | 12.4 | 7.2 ± 0.2 | 0.5 ± 0.2 | 0 | 93.5 |
| 10 | $Co_5Cu_1Mn_1O_x(200)$ | 16.8 | 9.4 ± 0.3 | 0.8 ± 0.2 | 0.2 ± 0.2 | 84.7 |
| 11 | $Co_9Cu_1Mn_1O_x(200)$ | 18.9 | 10.1 ± 0.2 | 0.9 ± 0.2 | 0.7 ± 0.1 | 90.4 |
| 12 | $Co_1Cu_3Mn_1O_x(200)$ | 3.1 | 1.6 ± 0.2 | 0.3 ± 0.1 | 0 | 84.2 |
| 13 | $Co_1Cu_1Mn_3O_x(200)$ | 2.1 | 1.1 ± 0.2 | 0.2 ± 0.1 | 0 | 84.6 |
| 14[c] | $Co_7Cu_1Mn_1O_x(200)$ | 28.4 | 15.1 ± 0.2 | 1.3 ± 0.1 | 1.2 ± 0.1 | 85.8 |
| 15 | $Co_7Cu_{0.25}Mn_{1.75}O_x(200)$ | 13.6 | 7.7 ± 0.1 | 0.4 ± 0.2 | 0.4 ± 0.1 | 90.6 |
| 16 | $Co_7Cu_{0.75}Mn_{1.25}O_x(200)$ | 22.9 | 12.7 ± 0.2 | 0.7 ± 0.1 | 0.9 ± 0.1 | 88.8 |
| 17 | $Co_7Cu_{1.25}Mn_{0.75}O_x(200)$ | 24.0 | 11.5 ± 0.2 | 2.6 ± 0.1 | 0.9 ± 0.1 | 76.7 |
| 18 | $Co_7Cu_{1.75}Mn_{0.25}O_x(200)$ | 14.1 | 5.0 ± 0.1 | 2.5 ± 0.1 | 1.3 ± 0.1 | 56.8 |

[a] Reaction conditions: catalyst 50 mg, $CO_2/H_2/N_2$ 10%/30%/60%, full irradiation, 200 °C, 3 h. [b] Detected by GC and obtained from three successive runs. [c] $N_2$ was replaced by Ar.

hydrocarbons than those of the pure $CoO_x(200)$ and $CuO_x(200)$ catalysts, indicating that the Cu species could not only enhance the activity of the Co-based catalyst in $CO_2$ reduction to $CH_4$, but also promote the formation of $C_{2+}$ products. For comparison, other trimetallic catalysts with different ratios were also assessed; however, all of them possessed lower activities than that of the $Co_7Cu_1Mn_1O_x(200)$ catalyst (entries 8 *vs.* 9–13).

The activities achieved in $CO_2/H_2/N_2$ and $CO_2/H_2/Ar$ were very similar (entries 8 *vs.* 14), indicating that the catalytic performances were not affected by the type of diluent gas. In addition, the $C_{2+}$ activities of the $Co_9Cu_1Mn_1O_x(200)$, $Co_7Cu_1Mn_1O_x(200)$, $Co_5Cu_1Mn_1O_x(200)$, and $Co_3Cu_1Mn_1O_x(200)$ catalysts were only 0.9, 1.4, 0.8, and 0.5 mmol $g_{cat}^{-1}$ $h^{-1}$, respectively, and inconsistent with the change rule of the catalyst composition. Because the formation of $C_{2+}$ products is closely related to the Cu species, the uneven distribution of Cu species on the catalyst surface is probably the reason for the discrepancy between the $C_{2+}$ activity and the Co/Cu/Mn molar ratio of the catalyst.

The Co species are the active sites; however, the promoters of Cu and Mn species are also very important for the reaction. To confirm this, the catalysts with the same component of Co element were investigated, and the results indicated that the Cu and Mn concentrations affected the catalytic performances remarkably (entries 15–18). The $Co_7Cu_{0.75}Mn_{1.25}O_x(200)$ and $Co_7Cu_{1.25}Mn_{0.75}O_x(200)$ catalysts showed high $CH_4$ formation activities, while the $Co_7Cu_{0.25}Mn_{1.75}O_x(200)$ and $Co_7Cu_{1.75}Mn_{0.25}O_x(200)$ catalysts offered relatively low values, indicating that the low concentrations of Cu and Mn are not beneficial for catalysis.

The catalytic performance studies showed that the coexistence of Co, Cu, and Mn in the Co/Cu/Mn trimetal is very important for the reaction, and their molar ratios and the synergistic effects of these multicomponents are closely related to the catalytic performances, and a similar phenomenon could be found in the previous report.[42]

### Effect of the reduction temperature of the $Co_7Cu_1Mn_1O_x$ catalysts

The above characterization results indicated that the reduction temperature affected the metal valence compositions of the catalysts, and it was proved to be able to affect their catalytic performances.[43,44] To verify this, the catalysts reduced at different temperatures were studied, and the results are shown in Fig. 4. Indeed, the $Co_7Cu_1Mn_1O_x$ and $Co_7Cu_1Mn_1O_x(100, 200, \text{and } 300)$ catalysts showed good catalytic performances during the reaction, indicating that they have similar catalyst

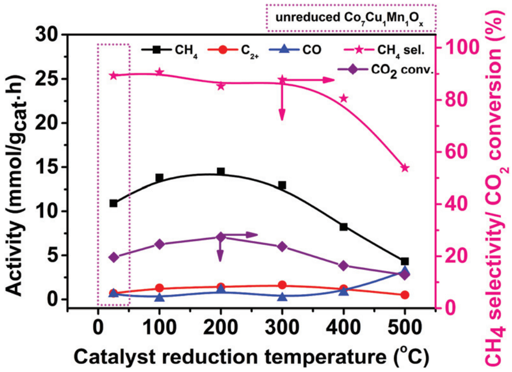

**Fig. 4** Effect of the reduction temperature of the $Co_7Cu_1Mn_1O_x(T)$ catalysts on the catalytic performances of photothermal $CO_2$ reduction. Reaction conditions: catalyst 50 mg, $CO_2/H_2/N_2$ 10%/30%/60%, 200 °C, 3 h, and 300 W Xe lamp full irradiation.

compositions and properties. However, the $Co_7Cu_1Mn_1O_x$(400 and 500) catalysts showed decreased catalytic activities, which has a great relationship with the high concentration of $Co^0$ in the bulk phase but less $Co_3O_4$ and $Mn_2O_3$.

The catalysts after being used for 9 h and 21 h were characterized by XPS and XRD in Fig. 5, and the results showed that $Co^0$ and $Cu^0$ species could be found during the reaction. $Co^0$ was widely recognized as the active site for $CO_2$ hydrogenation. The XRD patterns of the catalysts used for 9 h showed similar peaks to those of $Co_3O_4$ and CoO, revealing that $Co_3O_4$ still exists in the bulk phase. Compared with the $Co_7Cu_1Mn_1O_x$(200) catalyst in Fig. 2, the peak at 36.6° decreased remarkably. The catalyst used for 21 h showed similar results but with more $Co^0$ and $Cu^0$ species. The XPS and XRD characterization studies showed that the catalyst compositions were stable during the reaction.

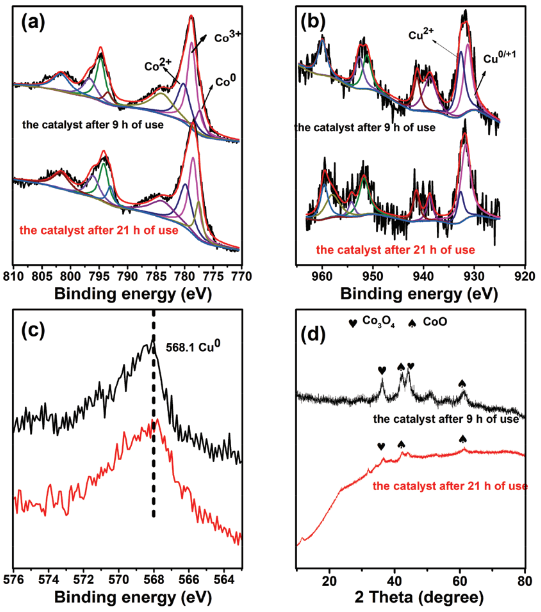

**Fig. 5** XPS tests (a, Co 2p; b, Cu 2p; c, Cu 3s LMM AES) and XRD pattern (d) for the catalysts after 9 h and 21 h of uses, respectively.

The highest $CH_4$ activity was achieved over the $Co_7Cu_1Mn_1O_x$(200) catalyst. Besides, the $Co_7Cu_1Mn_1O_x$(100 and 300) catalysts also showed acceptable $CH_4$ formation activities. Generally, in thermal catalysis, $Co^0$ species are recognized as the active components. However, the $Co_7Cu_1Mn_1O_x$(500) catalyst showed the lowest activity in the reaction, which mainly contained the $Co^0$ species but no $Co_3O_4$ or $Mn_2O_3$. It should be noted that in the present photothermal catalysis, the oxides including $Co_3O_4$, $Mn_2O_3$, *etc.* could promote the reaction *via* the interaction effect between the Co species and other oxides.

The $H_2$-TPR tests were carried out to study the interaction effect of different metal oxides, and the results are shown in Fig. 6. Pure $Co_3O_4$ showed two peaks at 273 °C and 336 °C, which could be assigned to the reduction peaks of $Co_3O_4$ to CoO and CoO to $Co^0$, respectively.[46] $Mn_2O_3$ showed two peaks located at 292 °C and 388 °C, which could be assigned to the reduction of $Mn_2O_3$ to $Mn_3O_4$ and $Mn_3O_4$ to MnO, respectively.[47,48] The $Co_7Cu_1O_x$ catalyst had two peaks at lower temperatures of 156 °C and 210 °C indicating that Cu could obviously promote the reduction of $Co_3O_4$ and CoO, which is consistent with previous reports.[45] However, the $Co_7Mn_1O_x$ catalyst showed two main peaks at 280 °C and 428 °C, which could be assigned to the reduction of $(Co,Mn)_3O_4$ to (Co,Mn)O, and (Co,Mn)O to $Co^0$ and MnO,[5,49,50] respectively, revealing that Mn species impedes the reduction of $CoO_x$. The $Co_7Cu_1Mn_1O_x$ catalyst had three peaks at 128, 183, and 284 °C, which could be attributed to the reduction peaks of CuO to $Cu^0$, $Co_3O_4$ to CoO, and CoO to $Co^0$ and MnO, respectively.[50] The $H_2$-TPR results indicated that the Co, Cu, and Mn species show strong interaction effects, and the previous report showed that the presence of Cu could alter the electronic interactions with Co and Ni in the Co–Cu–Ni trimetallic catalysts.[30]

The surface adsorption capacities could significantly affect the catalytic activity. Thus, we conducted the $CO_2$-TPD and $H_2$-TPD tests for the diverse trimetallic catalysts and the results indicated that with the increase of the reduction temperature, the adsorption amounts of $CO_2$ and $H_2$ on the catalysts decreased. The $Co_7Cu_1Mn_1O_x$(100 and 200) catalysts contained higher $CO_2$ and $H_2$ adsorption amounts than the others,

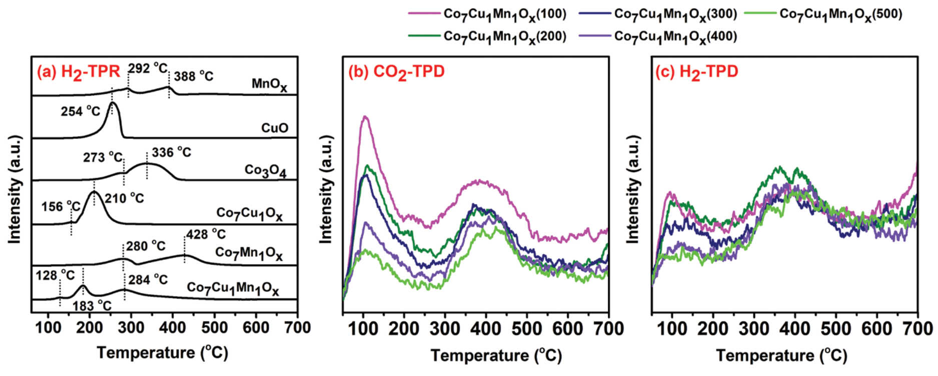

**Fig. 6** $H_2$-TPR(a), $CO_2$-TPD (b), and $H_2$-TPD (c) tests for the different catalysts.

which is beneficial for them to catalyze the $CO_2$ photothermal reduction.

To investigate the effects of the Mn and Cu species on the Co-based catalysts, the $CO_2$-TPD tests for Co–Mn and Co–Cu bimetallic catalysts were performed (Fig. S7†). The Mn species was found to be able to improve $CO_2$ and $H_2$ adsorption for the Co-based catalysts, while the Cu species reduced their adsorption since the Co–Cu bimetallic catalyst could be deeply reduced at 200 °C. Even so, the $Co_7Cu_1O_x(200)$ catalyst exhibited a strong $CO_2$ adsorption peak at around 350 °C, showing that the Cu species could promote strong adsorption of $CO_2$ on the catalyst.

We investigated the catalytic performances of the Co–Cu and Co–Mn bimetallic catalysts reduced at different temperatures, and the results are given in Table S4.† With the increase of the reduction temperature, the activities of the Co–Cu and Co–Mn catalysts increased initially but were then reduced at high reduction temperatures of 400 and/or 500 °C. The highest activities were lower than that of the $Co_7Cu_1Mn_1O_x(200)$ catalyst (Table 1, entry 8), indicating that the Cu and Mn species were both needed for the photothermal $CO_2$ reduction.

## Effect of the reaction conditions

The above investigation showed the composition and pretreatment of the catalyst affected the activity remarkably. In addition, the reaction conditions also had a great influence on the catalytic performance. The effects of the reaction conditions on the catalytic performance were also investigated, and the results are shown in Fig. 7. Almost no product was detected in the absence of $CO_2$ or $H_2$, indicating that the products are generated from $CO_2$. This was further confirmed by a control experiment of adding $^{13}CO_2$ in the reaction, in which $^{13}CH_4$ was detected with a mass spectrometer (Fig. S8†).

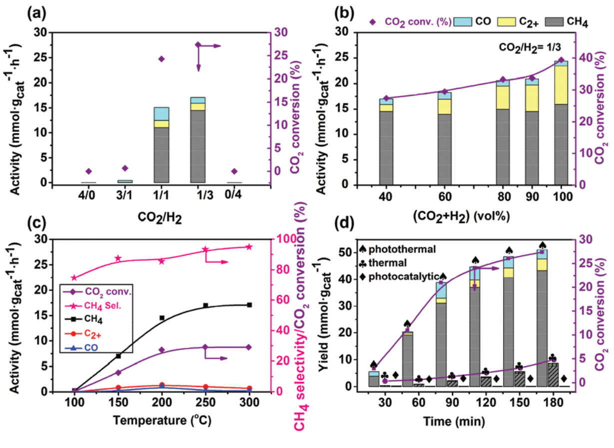

Fig. 7 Effects of the reaction conditions on the catalytic performances of photothermal $CO_2$ reduction over the $Co_7Cu_1Mn_1O_x(200)$ catalyst; (a) effect of the $CO_2/H_2$ ratio, (b) effect of the total concentration of $CO_2$ and $H_2$, (c) effect of the reaction temperature, and (d) effect of the reaction time. Reaction conditions: catalyst 50 mg, 300 W Xe lamp full irradiation and (a) $(CO_2 + H_2)/N_2$ 40%/60%, 200 °C, 3 h; (b) $CO_2/H_2$ 1/3, 200 °C, 3 h; (c) $CO_2/H_2/N_2$ 10%/30%/60%, 3 h; and (d) $CO_2/H_2/N_2$ 10%/30%/60%, 200 °C, spades (♠) photothermal conditions, clubs (♣) thermal conditions, and diamonds (◆) photocatalytic conditions respectively.

The best performances for $CH_4$ formation were achieved in $CO_2/H_2$ with a molar ratio of 1/3 (Fig. 6a). Surprisingly, changing the $CO_2$ and $H_2$ concentrations slightly affected the activity of $CH_4$ formation (around 15 mmol $g_{cat}^{-1}$ $h^{-1}$), but had an influence on $C_{2+}$ hydrocarbon formation. In the absence of a dilute gas, the highest $C_{2+}$ activity reached 7.5 mmol $g_{cat}^{-1}$ $h^{-1}$ with a 30.8% selectivity. Generally, $C_{2+}$ hydrocarbon formation involves $CO_2$ reduction and C–C coupling steps, and is much more difficult to achieve under photothermal conditions.[51] Thus, the present $Cu_7Cu_1Mn_1O_x(200)$ catalyst could catalyze the $C_{2+}$ hydrocarbon formation, but only the $CO_2$ and $H_2$ concentrations need to be enhanced. The $C_{2+}$ formation is strongly linked to the amount of surface adsorbed carbon species such as CO, $-CH_2-$, *etc.* A high amount of carbon species can be coupled to generate $C_{2+}$ hydrocarbons over a suitable catalyst, thus an increase of the $CO_2$ concentration could enhance the $C_{2+}$ selectivity. However, generally, to obtain $C_{2+}$ products, high pressure and/or $CO_2/H_2$ molar ratio are always needed.[42] The present $Co_7Cu_1Mn_1O_x(200)$ catalyst has a good $CO_2$ adsorption capacity, which was confirmed by the $CO_2$-TPD tests. The high $C_{2+}$ selectivity indicates that the $Co_7Cu_1Mn_1O_x(200)$ catalyst possesses good $CO_2$ reduction and C–C coupling abilities even under ambient pressure and a low $CO_2/H_2$ molar ratio (1/3). These multi-functional applications of synthesis of $CH_4$ and $C_{2+}$ hydrocarbons stemmed from the multiple interfaces created by the complicated compositions of $Co^0$, $Co_3O_4$, $Mn_2O_3$, CuO and $Cu_2O$ species, *etc.*

The reaction temperature has a significant influence on the catalytic performance, which was monitored using a thermocouple positioned above the catalyst level (Fig. S6†). As shown in Fig. 7c, high temperature promoted the reaction remarkably. With the increase of the reaction temperature, the activity of $CH_4$ formation increased. The $C_{2+}$ selectivity increased initially and then slightly decreased at a temperature higher than 200 °C. This is probably because at high temperature, the catalyst was sintered and reduced, which affected the product distribution especially with the $CH_4$ selectivity increased and $C_{2+}$ products decreased.

The evolution of activity on reaction time was also studied and the results are shown in Fig. 7d. In the first 30 min of reaction, $CH_4$ was formed with a very low activity, indicating that the catalyst had an induction period. During this period, the surface Co species, especially the surface CoO was reduced to the active $Co^0$ species. With prolonged time, the $CH_4$ formation activity increased remarkably. During our experiments, we found that the pressure of the reaction gas decreased remarkably after 3 h, but further prolonging the time did not show any remarkable decrease, indicating that the reaction has reached equilibrium. Thus, we chose 3 h as the optimum reaction time. In addition, control experiments were conducted to investigate the effect of optical and thermal conditions. The reaction could hardly occur under light irradiation but without extra heating, and the sole thermal conditions offered a very low $CH_4$ formation activity (only one-sixth that of the photothermal reaction). However, their combination is beneficial for the $CO_2$ reduction, indicating that the excellent catalytic performances stemmed from their synergistic promotion effect.

As mentioned above, the present catalytic system could achieve the photothermal $CO_2$ reduction to $C_{2+}$ hydrocarbons, but only needs to enhance the concentrations of $CO_2$ and $H_2$ to 25% and 75%. Fig. S9† shows the catalytic performances of the reaction. Under the conditions of 200 °C and 3 h, the highest $C_{2+}$ selectivity and activity reached 30.8% and 7.5 mmol $g_{cat}^{-1}$ $h^{-1}$ obtained after 3 h of reaction.

The results indicated that the multifunctional applications of the trimetallic Co–Cu–Mn catalysts derive from not only the multicomponents of the catalysts, but also the interaction effects between the components.

### Photoelectric properties of the Co–Cu–Mn catalysts

The study of the catalytic performances confirmed that $Co_3O_4$ and $Mn_2O_3$ oxides are very important for the reaction, and this differs from the fully reduced Co-based catalysts in $H_2$ such as $Co/CoO_x$[29] and $Co_6/MnO_x$[5] catalysts in $CO_2$ thermal hydrogenation. This diversification is probably because photothermal catalysis needs more light-sensitive components such as $Co_3O_4$ and $Mn_2O_3$ due to their semiconductor nature,[52,53] while the thermal catalyst favours low-valent metals such as $Co^0$.

To further investigate the light-sensitive properties of the Co–Cu–Mn trimetallic catalysts, the UV-vis DRS spectra were investigated, and the results are shown in Fig. S10a.† The unreduced catalysts including $Co_7Mn_1O_x$, $Co_7Cu_1O_x$, and $Co_7Cu_1Mn_1O_x$ showed higher absorption than the corresponding reduced catalysts throughout the UV-vis region. This was because the former mainly contain $Co_3O_4$, which has strong absorption of d–d transitions.[54] Upon reduction, the $Co_3O_4$ amount decreased, leading to the decrease of absorption accordingly. As for the $Co_7Cu_1Mn_1O_x$(200, 300, 400, and 500) catalysts, with the increase of the reduction temperature, the absorption strength decreased gradually for the deep reduction of $Co_3O_4$ to CoO and $Co^0$ species. Both the $Co_7Cu_1O_x$(200) and $Co_7Cu_1Mn_1O_x$(500) catalysts showed a lower absorbance than the other samples because they did not contain the $Co_3O_4$ species, which was confirmed by the XRD tests.

The band gap energies ($E_g$) for the tested catalysts were calculated using the Kubelka–Munk (K–M) model.[55] The $Co_7Cu_1Mn_1O_x$(200) catalyst had a lower $E_g$ value (1.86 eV) than those of the catalysts reduced at higher temperatures (Fig. S10b†). The $Co_7Cu_1Mn_1O_x$(500) catalyst, however, had the highest $E_g$ (3.26 eV) value and showed a very low activity in the reaction. The low $E_g$ value of the $Co_7Cu_1Mn_1O_x$(200) catalyst led to the feature that the electrons in the semiconductor could be easily excited under light irradiation. The lower band gap is conducive to visible light excitation, which was confirmed by the control experiments using different types of light including full irradiation (300–1100 nm), UV (300–420 nm), and visible light (420–800 nm). The catalytic performances obtained under visible light illumination are almost similar to those under UV-vis and full irradiation, as shown in Table S5.†

The photocurrent–time curves of the $Co_7Cu_1Mn_1O_x$(100, 200, 300, and 400) catalysts are shown in Fig. S10c.† All of these catalysts showed obvious photocurrent response behavior, indicating that they could be excited to generate electron–hole pairs.

$Co_3O_4$, $Mn_2O_3$, $Cu_2O$, and CoO are p-type semiconductors; however, after reduction, oxygen vacancies were created and regulated the p-type to a n-type semiconductor, which is confirmed by the Mott–Schottky curves shown in Fig. S10d.† All the catalysts showed dipolar (p-type and n-type) semiconductor properties, resulting from the multiple interfaces of the complex trimetallic catalyst.

The EIS Nyquist plots of the tested samples including $Co_7Cu_1Mn_1O_x$(100, 200, 300, and 500) showed similar arc radii, revealing that they have similar impedance values and electron transfer rates (Fig. S10e†).[56]

The photothermal effect was investigated *via* testing the stable temperature of the samples under vacuum (Fig. S11†). Under similar conditions, the catalyst temperatures were monitored using an infrared camera. Among the tested catalysts, the $MnO_x$ catalyst showed the highest temperature (104.6 °C) under the full irradiation, while the $CuO_x$ catalyst offered the lowest (88.3 °C). The $Co_7Cu_1Mn_1O_x$(200) catalyst showed a higher temperature (102.2 °C) than that of the $Co_7Cu_1Mn_1O_x$(500) (95.8 °C), indicating that the $Co_7Cu_1Mn_1O_x$(200) catalyst could provide a higher local heating environment. The results revealed that the presence of Mn could provide a higher local temperature for the catalyst.

In summary, the results obtained due to the photoelectrical characteristics indicated that the $Co_7Cu_1Mn_1O_x$(200) catalyst is a p-type and n-type semiconductor, showing a low band gap. All of these properties are closely related to the excellent catalytic activity in photothermal $CO_2$ reduction. However, it should be noted that the unique catalytic performances of the $Co_7Cu_1Mn_1O_x$(200) catalyst were derived from the synergistic effect of the adsorption effect, light-response properties, and photothermal effect.

### Light effect and the proposed mechanism for photothermal $CO_2$ reduction

In the present catalytic system, the synergistic effect between light and heat had a great influence on the catalytic activity. Under light irradiation, the electrons of the $Co_7Cu_1Mn_1O_x$(200) catalyst could be excited to generate the electron–hole pairs. Generally, in photocatalysis, the excited electrons and holes can participate in reactions.[57] However, under photothermal conditions, the $E_g$ value of the semiconductor is normally found to be lower, and the excited electrons recombine more easily with the photogenerated holes than under the traditional photocatalysis without heating.

To investigate the effects of the generated electron–hole pairs, we carried out two control experiments by adding sacrificial electron donors including *p*-xylene (~2.18 V *vs.* $Ag/AgCl_{sat}$) and anisole (1.92 V *vs.* $Ag/AgCl_{sat}$) in the absence of $H_2$.[18,25] As shown in Fig. S12,† both the reactions gave a very low $CH_4$

yield despite the fact that *p*-xylene and anisole could quench the photogenerated holes more efficiently than $H_2$. These results indicated that photocatalysis plays a minor role in the present photothermal $CO_2$ reduction. In this aspect, similar to the Ru-,[18] Rh-,[58] Au-,[58] and Ag-based[59] catalysts, the charge separation and recombination under light irradiation resulted in a local thermal effect at the surface of the catalyst, offering more energy to promote $CO_2$ reduction.

The mechanism for the photothermal $CO_2$ reduction to hydrocarbons is still unclear, and two reaction routes are generally accepted.[60] The first involves a CO intermediate, in which $CO_2$ is initially converted to CO, and CO could be further hydrogenated to hydrocarbons.[61] The other route is the direct $CO_2$ conversion. In this route, $CO_2$ is hydrogenated to carbonate, formate, and methoxy intermediates, and then hydrogenated to hydrocarbons. In this work, the CO formation activity was very low. To study the reaction pathway, we conducted the control experiments of replacing $CO_2$ by CO under the conditions given in Table 1, entry 8. Interestingly, the activities of $CH_4$ and $C_{2+}$ were 4.9 and 7.3 mmol $g_{cat}^{-1}$ $h^{-1}$, and their selectivities were 40.2% and 59.8%, respectively (Table 1, entry 8, Fig. S13, S14 *vs.* Table S6, entry 2, Fig. S15†). To exclude that the high CO concentration may occupy the active sites on the catalyst surface, a mixed gas of 2%CO/8%$CO_2$ (total 10%) was also reacted (Table S6, entry 3 and Fig. S16†). However, the activities of $CH_4$ and $C_{2+}$ were 7.2 and 2.8 mmol $g_{cat}^{-1}$ $h^{-1}$ with the selectivities of 72.0% and 28.0%, respectively. The results implied that the presence of CO could not improve but reduce the $CH_4$ activity, meaning that in the photothermal $CO_2$ reduction, $CH_4$ is probably not formed *via* the CO intermediate route. However, CO was found to be beneficial for the $C_{2+}$ synthesis, revealing that it is probably an intermediate for the formation of the $C_{2+}$ hydrocarbon product.

The characterization results confirmed that the trimetallic $Co_7Cu_1Mn_1O_x$(200) catalyst contains CoO, $Co_3O_4$, $Cu_2O$, $Mn_2O_3$, *etc*. During the reaction, the CoO species could be reduced to $Co^0$, which was recognized as the active site. The CoO and $Cu_2O$ species could be reduced by $H_2$ to $Co^0$ and $Cu^0$ during the reaction, which was confirmed by the XPS results (Fig. 5). In the present photothermal $CO_2$ hydrogenation, metal oxides such as $Co_3O_4$ and $Mn_2O_3$ were very important for the reaction because they are semiconductors, which could generate electrons and holes under light illumination. A quick recombination of electrons and holes provides a local heating environment for the catalysts, and further promotes the reaction.[5] In addition, $Mn_2O_3$ could offer Lewis acidic sites to enhance $CO_2$ and $H_2$ adsorption capacity of the catalyst.

Cu species could promote the partial reduction of cobalt oxides to CoO and $Co^0$ and maintain the presence of CoO and $Co_3O_4$ prior to and during the reaction, and reduce the temperature of catalyst reduction. Besides, the $CO_2$-TPD tests and the control experiments confirmed that the Cu species or the Cu–Co interfaces could provide strong $CO_2$ adsorption sites to convert $CO_2$ to CO, and further form $C_{2+}$ hydrocarbons.

It should be mentioned that, although $CH_4$ was probably not formed *via* the CO route, CO could be produced with an activity of 1.1 mmol $g_{cat}^{-1}$ $h^{-1}$ (entry 8, Table 1). Importantly, the higher concentration of CO could make it easily coupled into the $C_{2+}$ products over the same $Co_7Cu_1Mn_1O_x$(200) catalyst. Thus, $C_{2+}$ hydrocarbons could be formed by increasing the $CO_2$ concentration.

In addition, the present protocol could be extended to photothermal CO hydrogenation. We conducted the reaction over the $Co_7Cu_1Mn_1O_x$(200) catalyst under the similar conditions given in Table 1, entry 8, and the results are shown in Fig. S17.† The photothermal activity is about 7 times higher than that of the thermal activity, and the selectivity of the $C_{2+}$ products is higher than that of $CH_4$, which is similar to $CO_2$ hydrogenation. The results indicated that the present trimetallic Co–Cu–Mn catalyst has multifunctional applications as shown in photothermal CO hydrogenation.

## The reusability and stability studies of the $Co_7Cu_1Mn_1O_x$(200) catalyst

The reusability of the $Co_7Cu_1Mn_1O_x$(200) catalyst was investigated, and the results are shown in Fig. 8a. For comparison, the $CO_2$ reduction reactions were alternatively conducted under photothermal and thermal conditions. The results revealed that the present catalyst possesses good reusability in the reaction, and after using for 18 times, it still offered an activity of higher than 10 $mmol_{CH_4}$ $g_{cat}^{-1}$ $h^{-1}$. Besides, the results also confirmed that the activities under photothermal conditions were much higher than those under thermal conditions. The used catalysts were characterized by XRD and XPS, and the results are shown in Fig. 5, respectively.

The activity loss is probably caused by catalyst agglomeration, which was confirmed by the TEM images of the catalyst after being used 18 times (Fig. S18).† The size of the used catalyst increased in the range 40–90 nm.

Fig. 8b shows the temporal stability of the $Co_7Cu_1Mn_1O_x$(200) catalyst in a continuous flow operation (details are given in the ESI†). The catalyst offered approximately 20 mmol $g_{cat}^{-1}$ $h^{-1}$ of $CH_4$ after a short induction period of 3 h, and maintained higher than 18 mmol $g_{cat}^{-1}$ $h^{-1}$

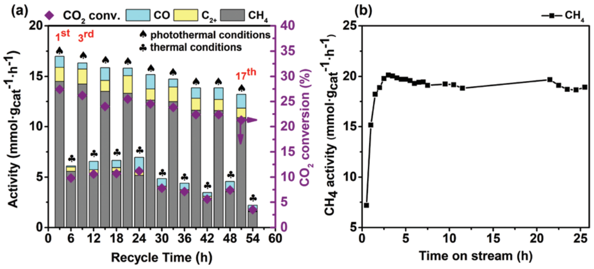

**Fig. 8** Reusability (a) and temporal stability (b) studies of $Co_7Cu_1Mn_1O_x$(200) in photothermal $CO_2$ reduction. Reaction conditions: (a) catalyst 50 mg, 200 °C, $CO_2/H_2/N_2$ 10%/30%/60%, full irradiation for photothermal conditions; (b) catalyst 50 mg, 200 °C, $CO_2/H_2/N_2$ 10%/30%/60% 20 mL $min^{-1}$, full irradiation.

even after 25 hours of reaction. The result showed that the present $Co_7Cu_1Mn_1O_x$(200) catalyst has a long-term temporal stability, confirming that it has a potential industrial application.

## Conclusions

In summary, a trimetallic Co–Cu–Mn catalytic system for photothermal $CO_2$ reduction was constructed by a simple co-precipitation method. The metal compositions and reduction temperatures of the catalysts affected their activities remarkably, and the screened $Co_7Cu_1Mn_1O_x$(200) catalyst could offer 14.5 mmol $g_{cat}{}^{-1}$ $h^{-1}$ of $CH_4$ at low $CO_2$ (10%) and $H_2$ (30%) concentrations. Importantly, the catalyst system could produce $C_{2+}$ hydrocarbons with an activity of 7.5 mmol $g_{cat}{}^{-1}$ $h^{-1}$ and a selectivity of 30.8% by only improving the $CO_2$ and $H_2$ concentrations to 25% and 75%, respectively. High activities stemmed from the multicomponents of the catalyst, especially the metallic $Co^0$, $Cu^0$, and CoO, $Co_3O_4$, $Cu_2O$, and $Mn_2O_3$ semiconductors. The Cu species could tune the reduction characteristics, and further tune the balance of $Co^{2+}$ and $Co^{3+}$. The Mn species could enhance the $CO_2$ and $H_2$ adsorption, and also offer a high local temperature for the nanocatalyst. The present strategy of partial reduction of the Co–Cu–Mn trimetallic catalyst not only highlights the route for using solar energy to produce valuable chemicals under mild conditions especially low $CO_2$ concentration, but also constructs the highly efficient trimetallic catalysts with multifunctional applications in photothermal catalysis.

## Conflicts of interest

There are no conflicts to declare.

## Acknowledgements

The authors gratefully acknowledge the financial supports from the National Natural Science Foundation of China (21978160, 21776170, 22078182, 21706152, and 21908139), the Natural Science Basic Research Plan in Shaanxi Province of China (Program No. 2019JLM-16, 2019JQ-772, and 2019JQ-782) and the Key Industrial Innovation Project of Shaanxi Provincial Science and Technology Department (2019ZDLGY06-04).

## Notes and references

1 M. He, Y. Sun and B. Han, *Angew. Chem., Int. Ed.*, 2013, **52**, 9620–9633.
2 L. Wang, Y. Dong, T. Yan, Z. Hu, A. A. Jelle, D. M. Meira, P. N. Duchesne, J. Y. Y. Qiu, E. E. Storey, Y. Xu, W. Sun, M. Ghoussoub, N. P. Kherani, A. S. Helmy and G. A. Ozin, *Nat. Commun.*, 2020, **11**, 2432.
3 B. Zhou, P. Ou, N. Pant, S. Cheng, S. Vanka, S. Chu, P. T. Rashid, G. Botton, J. Song and Z. Mi, *Proc. Natl. Acad. Sci. U. S. A.*, 2020, **117**, 1330–1338.
4 M. Cui, Q. Qian, J. Zhang, Y. Wang, B. B. A. Bediako, H. Liu and B. Han, *Chem*, 2021, **7**, 726–737.
5 Z. He, M. Cui, Q. Qian, J. Zhang, H. Liu and B. Han, *Proc. Natl. Acad. Sci. U. S. A.*, 2019, **116**, 1254–12659.
6 Z. Ma and M. D. Porosoff, *ACS Catal.*, 2019, **9**, 2639–2656.
7 R. De, S. Gonglach, S. Paul, M. Haas, S. S. Sreejith, P. Gerschel, U.-P. Apfel, T. H. Vuong, J. Rabeah, S. Roy and W. Schöfberger, *Angew. Chem., Int. Ed.*, 2020, **59**, 10527–10534.
8 Y. Wang, X. Shang, J. Shen, Z. Zhang, D. Wang, J. Lin, J. C. S. Wu, X. Fu, X. Wang and C. Li, *Nat. Commun.*, 2020, **11**, 3043.
9 A. Weihard, S. P. Argent and V. Sans, *Nat. Commun.*, 2021, **12**, 231.
10 Z. He, Q. Qian, J. Ma, Q. Meng, H. Zhou, J. Song, Z. Liu and B. Han, *Angew. Chem., Int. Ed.*, 2016, **55**, 737–741.
11 L. Wang, E. Guan, Y. Wang, L. Wang, Z. Gong, Y. Cui, X. Meng, B. C. Gates and F.-S. Xiao, *Nat. Commun.*, 2020, **11**, 1033.
12 M. Rahaman, K. Kiran, I. Z. Montiel, V. Grozovski, A. Dutta and P. Broekmann, *Green Chem.*, 2020, **22**, 6497–6509.
13 G. Chen, R. Gao, Y. Zhao, Z. Li, G. I. N. Waterhouse, R. Shi, J. Zhao, M. Zhang, L. Shang, G. Sheng, X. Zhang, X. Wen, L.-Z. Wu, C.-H. Tung and T. Zhang, *Adv. Mater.*, 2017, 1734663.
14 F. Sastre, A. V. Puga, L. Liu, A. Corma and H. García, *J. Am. Chem. Soc.*, 2014, **136**, 6798–6801.
15 J. Albero, E. Dominguez, A. Corma and H. Garcia, *Sustain. Energy Fuels*, 2017, **7**, 1303–1307.
16 F. Zhang, Y.-H. Li, M.-Y. Qi, Y. M. A. Yamada, M. Anpo, Z.-R. Tang and Y.-J. Xu, *Chem. Catal.*, 2021, **1**, 1–26.
17 P. G. O'Brien, A. Sandhel, T. E. Wood, A. A. Jelle, L. B. Hoch, D. D. Perovic, C. A. Mims and G. A. Ozin, *Adv. Sci.*, 2014, **1**, 1400001.
18 D. Mateo, J. Albero and H. García, *Joule*, 2019, **3**, 1–14.
19 A. A. Jelle, K. K. Ghuman, P. G. O'Brien, M. Hmadeh, A. Sandhel, D. D. Perovic, C. V. Singh, C. A. Mims and G. A. Ozin, *Adv. Energy Mater.*, 2018, **8**, 1702277.
20 J. Ren, S. Ouyang, H. Xu, X. Meng, T. Wang, D. Wang and J. Ye, *Adv. Energy Mater.*, 2016, 1601657.
21 X. Meng, T. Wang, L. Liu, S. Ouyang, P. Li, H. Hu, T. Kako, H. Iwai, A. Tanaka and J. Ye, *Angew. Chem., Int. Ed.*, 2014, **53**, 11478–11482.
22 C. Wang, S. Fang, S. Xie, Y. Zheng and Y. H. Hu, *J. Mater. Chem. A*, 2020, **8**, 7990–7394.
23 J. Jia, H. Wang, Z. Lu, P. G. O'Brien, M. Ghoussoub, P. Duchesne, Z. Zheng, P. Li, Q. Qiao, L. Wang, A. Gu, A. A. Jelle, Y. Dong, Q. Wang, K. K. Ghuman, T. Wood, C. Qian, Y. Shao, C. Qiu, M. Ye, Y. Zhu, Z.-H. Lu, P. Zhang, A. S. Helmy, C. V. Singh, N. P. Kherani, D. D. Perovic and G. A. Ozin, *Adv. Sci.*, 2017, 1700252.
24 M. Cabrero-Antonino, S. Remiro-Buenamañana, M. Souto, A. A. García-Valdivia, D. Choquesillo-Lazarte, S. Navalón, A. Rodríguez-Diéguez, G. M. Espallargas and H. García, *Chem. Commun.*, 2019, **55**, 10932–10935.

25 D. Mateo, J. Albero and H. García, *Energy Enviorn. Sci.*, 2017, **10**, 2392–2400.

26 M.-P. Jiang, K.-K. Huang, J.-H. Liu, D. Wang, Y. Wang, X. Wang, Z.-D. Li, X.-Y. Wang, Z.-B. Geng, X.-Y. Hou and S.-H. Feng, *Chem*, 2020, **6**, 2335–2346.

27 J. A. Rodriguez, P. Liu, D. J. Stacchiola, S. D. Senanayake, M. G. White and J. G. Chen, *ACS Catal.*, 2015, **5**, 6696–6706.

28 R. Lang, X. Du, Y. Huang, X. Jiang, Q. Zhang, Y. Guo, K. Liu, B. Qiao, A. Wang and T. Zhang, *Chem. Rev.*, 2020, **120**, 11986–12043.

29 K. Zhao, M. Calizzi, E. Moioli, M. Li, A. Borsay, L. Lombardo, R. Mutschler, W. Luo and A. Zuttel, *J. Energy Chem.*, 2021, **53**, 241–250.

30 M. Ao, G. H. Pham, V. Sage, V. Pareek and S. Liu, *Fuel Process. Technol.*, 2019, **193**, 141–148.

31 Y. Xiang, R. Barbosa, N. Kruse and X. Li, *ACS Catal.*, 2015, **5**, 2929–2934.

32 Y. Wang, S. Kattel, W. Gao, K. Li, P. Liu, J. G. Chen and H. Chen, *Nat. Commun.*, 2019, **10**, 1166.

33 A. A. S. Goncalves, P. B. Faustino, J. M. Assaf and M. Jaroniec, *ACS Appl. Mater. Interfaces*, 2017, **9**, 6079–6092.

34 Y. Li, H. S. Pillai, J. Lattimer, N. M. Adli, S. Karakalos, M. Chen, L. Guo, H. Xu, J. Yang, D. Su, H. Xin and G. Wu, *ACS Catal.*, 2020, **10**, 3945–3957.

35 M. Sharma, J.-H. Jang, D. Y. Shin, J. A. Kwon, D.-H. Lim, D. Choi, H. Sung, J. Jang, S.-Y. Lee, K. Y. Lee, H.-Y. Park, N. Jung and S. J. Yoo, *Energy Environ. Sci.*, 2019, **12**, 2200–2211.

36 L. Martin, H. Martinezz, D. Poinot, B. Pecquenard and F. L. Cras, *J. Phys. Chem. C*, 2013, **117**, 4421–4430.

37 Z. Geng, Y. Wang, J. Liu, G. Li, L. Li, K. Huang, L. Yuan and S. Feng, *ACS Appl. Mater. Interfaces*, 2016, **8**, 27825–27831.

38 L. Lukaskuk, N. Yigit, R. Rameshan, E. Kolar, D. Teschner, M. Havecker, A. Knop-Gericke, R. Schlogl, K. Fottinger and G. Rupprechter, *ACS Catal.*, 2018, **8**, 8630–8641.

39 J. Su, Z. Zhang, D. Fu, X. Xu, B. Shi, X. Wang, R. Si, Z. Jiang, J. Xu and Y. Han, *J. Catal.*, 2016, **336**, 94–106.

40 B. Rivas-Murias and V. Salgueiriño, *J. Raman Spectrosc.*, 2017, **48**, 837–841.

41 X. Jiang, X. Nie, X. Guo, C. Song and J. G. Chen, *Chem. Rev.*, 2020, **120**, 7984–8034.

42 Y. Xiang, V. Chitry, P. Liddicoat, P. Felfer, J. Cairney, S. Ringer and N. Kruse, *J. Am. Chem. Soc.*, 2013, **135**, 7114–7117.

43 Z.-H. He, C.-S. Jiang, K. Wang, Z.-Y. Wang, N. Li, W.-T. Wang and Z.-T. Liu, *Catal. Today*, 2020, **356**, 579–588.

44 M. Tahir, B. Tahir, N. A. S. Amin and A. Muhammad, *Energy Convers. Manag.*, 2016, **119**, 368–378.

45 Z.-H. He, N. Li, K. Wang, W.-T. Wang and Z.-T. Liu, *Mol. Catal.*, 2019, **470**, 120–126.

46 O. A. Bulavchenko, E. Y. Gerasimov and T. N. Afonasenko, *Dalton Trans.*, 2018, **47**, 17153–17159.

47 W. Yang, Y. Peng, Y. Wang, Y. Wang, H. Liu, Z. Su, W. Yang, J. Chen, W. Si and J. Li, *Appl. Catal., B*, 2020, **278**, 119279.

48 W. Yang, S. Wang, K. Li, S. Liu, L. Gan, Y. Peng and J. Li, *Chem. Eng. J.*, 2019, **364**, 448–451.

49 C.-I. Ahn, D.-W. Jeong, J. M. Cho, H.-S. Na, W.-J. Jang, H.-S. Roh, J.-H. Choi, S.-H. Um and J.-W. Bae, *Microporous Mesoporous Mater.*, 2016, **221**, 204–211.

50 O. A. Bulavchenko, E. Y. Gerasimov and T. N. Afonasenko, *Dalton Trans.*, 2018, **47**, 17153–17159.

51 G. Chen, R. Gao, Y. Zhao, Z. Li, G. I. N. Waterhouse, R. Shi, J. Zhao, M. Zhang, L. Shang, G. Sheng, X. Zhang, X. Wen, L. Wu, T. Tung and T. Zhang, *Adv. Mater.*, 2018, **30**, 1704663.

52 J. Zhao, Z. Zhao, N. Li, J. Nan, R. Yu and J. Du, *Chem. Eng. J.*, 2018, **353**, 805–813.

53 Y. Zeng, H. Li, Y. Xia, L. Wang, K. Yin, Y. Wei, X. Liu and S. Luo, *ACS Appl. Mater. Interfaces*, 2020, **12**, 44608–44616.

54 Z. Li, J. Liu, Y. Zhao, R. Shi, G. I. N. Waterhouse, Y. Wang, L.-Z. Wu, C.-H. Tung and T. Zhang, *Nano Energy*, 2019, **60**, 467–475.

55 A. Umasadharshini, M. Bououdina, M. Venkateshwarlu, C. Manoharan and P. Dhamodharan, *Surf. Interfaces*, 2020, **19**, 100535.

56 Q. Wan, J. Zhang, B. Zhang, D. Tan, L. Yao, L. Zheng, F. Zhang, L. Lin, X. Cheng and B. Han, *Green Chem.*, 2020, **22**, 2750–2754.

57 N. Li, M. Liu, B. Yang, W. Shu, Q. Shen, M. Liu and J. Zhou, *J. Phys. Chem. C*, 2017, **121**, 2923–2932.

58 X. Zhang, X. Li, D. Zhuang, N. Q. Su, W. Yang, H. O. Everitt and J. Liu, *Nat. Commun.*, 2017, **8**, 14542.

59 P. Christopher, H. Xin and S. Linic, *Nat. Chem.*, 2011, **3**, 467–472.

60 B. Miao, S. S. K. Ma, X. Wang, H. Su and S. H. Chan, *Catal. Sci. Technol.*, 2016, **6**, 4048–4058.

61 B. Tahir, M. Tahir and N. S. Amin, *Energy Convers. Manage.*, 2015, **90**, 272–281.